Proceedings of
11th European Conference on Turbomachinery Fluid dynamics & Thermodynamics
ETC11, March 23-27, 2015, Madrid, Spain

PERFORMANCE MEASUREMENTS OF A FULL-STAGE CENTRIFUGAL PROCESS GAS COMPRESSOR TEST RIG

T. Rossbach - C. Rube* - M. Wedeking* - H. Franz** - P. Jeschke**

*Institute of Jet Propulsion and Turbomachinery
RWTH Aachen University
Templergraben 55, 52062 Aachen, Germany

**MAN Diesel & Turbo SE
Steinbrinkstr. 1, 46145 Oberhausen, Germany

ABSTRACT

The paper presents the first experimental performance data for a mid-stage centrifugal compressor test rig built at RWTH Aachen University. The results provide an analysis of the operational and loss behavior and will be published in an open test case for validating numerical methods.

The test rig was built to investigate the operational and loss behavior of a complete return channel in detail and is broadly introduced. The measurements described in this paper were designed based on numerical calculations. Further, the stage performance is analyzed based on a compressor map for design speed, supplemented by detailed measurements inside the diffusion system. The performance of the diffuser and the return channel are discussed separately. The significant influence of the return channel design on the overall stage efficiency and pressure build-up is emphasized. Additional angle measurements at the stage outlet provide details about the inflow to the potential next compressor stage.

NOMENCLATURE

avg	average	b	channel width	c	absolute velocity
c_D	dissipation coefficient	c_f	friction coefficient	C_p	pressure recovery
DP	design point	exp	experiment	f	error
h	enthalpy	m	number of parameters	M	Mach number
n	number of samples	NC	near choke	NS	near stall
p	pressure	r	radius	r_h	degree of reaction
Re	Reynold's number	t_p	student factor	T	temperature
u	circumferential velocity	$u_{\overline{\Phi}}$	uncertainty of Φ	$\dot{V}$	volume flow rate
$\overline{x}$	measured parameter	α	absolute flow angle	β	relative flow angle
ϵ	interpolation threshold	η_p	polytropic efficiency	ν	kinematic viscosity
Π	pressure ratio	ρ	density	φ_Stage	flow coefficient
Φ	defined quantity	Ψ_h	work input coefficient	Ψ_y	head coefficient

Subscripts

$1-5$	plane definitions	diff	diffuser	dyn	dynamic
DP	design point	i	control variable	$\mathrm{i,j}$	measurement planes
imp	impeller	in	inlet plane	inf	infinite blade number
m	meridional direction	n	normalized	out	outlet plane
r	random error	s	systematic error	slip	impeller slip
t	total conditions	therm	thermal	ts	total to static
tt	total to total	u	circumferential direction		

INTRODUCTION

The high pressure ratios required for the chemical industry often cannot be realized with only one compressor stage. Therefore, centrifugal compressors are typically single-shaft, multistage compressors of several rotors with a radial outflow. After leaving the rotor, the fluid passes the attached diffusion system consisting of a vaned or vaneless diffuser followed by a return apparatus. The diffuser decelerates the flow and thus leads to an increase in static enthalpy. Then the fluid is redirected radially inward by a U-bend before it flows through a vaned return channel, which aligns the flow for the next stage. A final L-turn directs the flow in the axial direction to the next rotor. The flow inside the diffusion system contains complex 3D-structures and secondary flows. Their characteristics are e.g. discussed based on experimental studies of the velocity distribution inside the U-bend and the return channel by Inoue and Koizumi (1983), Simon and Rothstein (1983), Rothstein (1984) and Rothstein and Gallus (1983) for different geometries. These investigations show that complex flow phenomena and their appearance are not fully understood. With a 5 to 10 percentage point loss in overall compressor efficiency (see Aalburg et al. (2011)), the flow inside the diffusion system remains the topic of numerous investigations. One of the main objectives of these in most cases numerical investigations are the return channel vanes. Since cylindrical profiles are usually used in industrial compressor stages, they have great potential for optimization. The aim is to provide a larger redirection while the losses decrease, so that the outer stage diameter can be decreased for nearly constant efficiency. This leads to smaller friction and pressure losses inside the diffuser.

The big difficulty in numerical computations is to choose the right turbulence model to solve the secondary flow phenomena inside the return channel vanes as is shown in Lenke (1999), Lenke and Simon (1999) and Lenke and Simon (1998). Even Reutter et al. (2011) and Hildebrandt (2011) conceded that their results could be improved by validating their turbulence modeling with measurements. This shows that experimental results are essential for optimizing the flow path. Simpson et al. (2008) and Schmitz et al. (2008) therefore described the buildup of a $90°$ cascade rig and the validation of the numerical setup based on the measurement data. Based on this work, smaller diffusion systems for small flow rates were developed, which were measured on a rotating test rig by Aalburg et al. (2008). The results show that a decrease in the outer stage diameter is possible while the efficiency is nearly constant. Since the measurements were performed for small flow rates, they are not applicable to machines with higher flow rates. The flow through narrow channels is dominated by boundary layer effects due to the higher relative boundary layer height that prevents the formation of most complex 3D flow phenomena occuring in higher channels with higher flow rates. The test rig at RWTH Aachen University was built to optimize the diffusion system of a radial compressor stage with flow rates up to $\varphi_{\mathrm{Stage}} = 0.18$. The results will be published in an open test case. This paper presents the first performance data and confirms their reliability.

EXPERIMENTAL SETUP

Compressor Test Rig

The Institute of Jet Propulsion and Turbomachinery is investigating the centrifugal stages of single-shaft, multistage compressors for industrial applications on one test rig. The test rig, designed and set up in close collaboration with MAN Diesel & Turbo SE, Oberhausen, consists of a single stage and was completed in January 2014.

The rig is intended to operate with various types of closed impellers and is equipped with a high flow rate stage in the current setup as shown in Figure 1. The compressor is powered by a 1600 kW asynchronous motor, which is coupled to a 12.5:1 ratio gear box with rotational speeds up to 18750 rpm. The test rig has a magnetic bearing system that significantly decreases friction losses and thus enables an accurate measurement of the mechanical work using a torque meter. The test section is a closed loop for high repeatability of the experiments and an independent variation of Reynolds and Mach

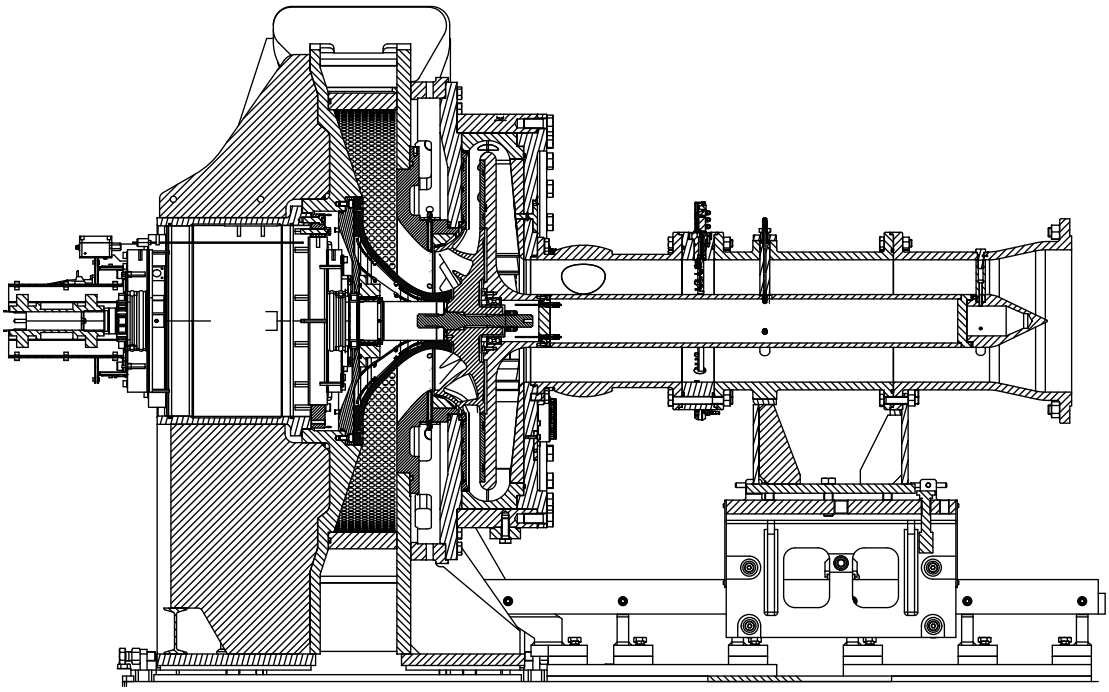

Figure 1: **Section view of the process compressor test rig**

numbers. The working fluid of the test rig is air. The air flows through a Venturi meter into a double-flow inlet system. A radial flow conditioner removes the inlet swirl and generates a circumferentially homogeneous flow field, which is accelerated toward the impeller eye. The axial extension of the inlet duct was increased for better accessibility of the impeller inlet plane. However, the duct is designed to generate an inlet flow profile similar to that of a narrower duct in a real machine.
The current rotor is a shrouded impeller with 15 three-dimensional blades, an outlet diameter of $d_2 = 0.4\,\mathrm{m}$, and a blade exit angle of $\beta_2 = 130°$. At design conditions, the rotor operates at a flow rate of $\varphi_{\mathrm{Stage}} = 0.15$, which is defined by

$$\varphi_{\mathrm{Stage}} = \frac{4\dot{V}}{\pi d_2^2 u_2} \quad , \tag{1}$$

and a circumferential Mach number of $M_{\mathrm{u2}} = 0.87$, which results in a moderate total pressure ratio of $\Pi_{\mathrm{tt}} = 1.57$. The impeller tip seal consists of five labyrinth seals in the casing with five corresponding steps on the cover disc of the impeller. The diffusion system of the investigated stage consists of a parallel-walled, vaneless diffuser, a cross-over bend, a vaned return channel, and a final L-turn. The large diffuser radius ratio of $r_4/r_2 = 1.75$ (see Figure 2) leads to strong mixing effects in the diffuser and weak interaction of the impeller and the return channel vanes. These mixing effects are enhanced by a shroud-sided pinch near the diffuser inlet that reduces the cross-sectional area of plane 3 by about 3% compared to the impeller exit plane (plane 2, see Figure 2). The cross section at the inlet and the exit of the cross-over bend are identical. Toward the top of the bend, the cross section is decreased as shown in Figure 2. This results in global acceleration of the flow toward the top and a deceleration towards the exit of the bend. The latter effect is strengthened near the hub by the additional deceleration caused by the transition from a convex curved to a straight wall. The 14 vanes of the return channel are cylindrical and have a thick leading edge for a wide incidence range. The cross section of the return channel is widened to approximately 162% of its inlet cross section (see Figure 2). The flow is turned in the front part of the channel whereas the rear part consists of straight planes and slightly accelerates the flow toward the L-turn. The L-turn itself is designed to guide the flow to the next stage.

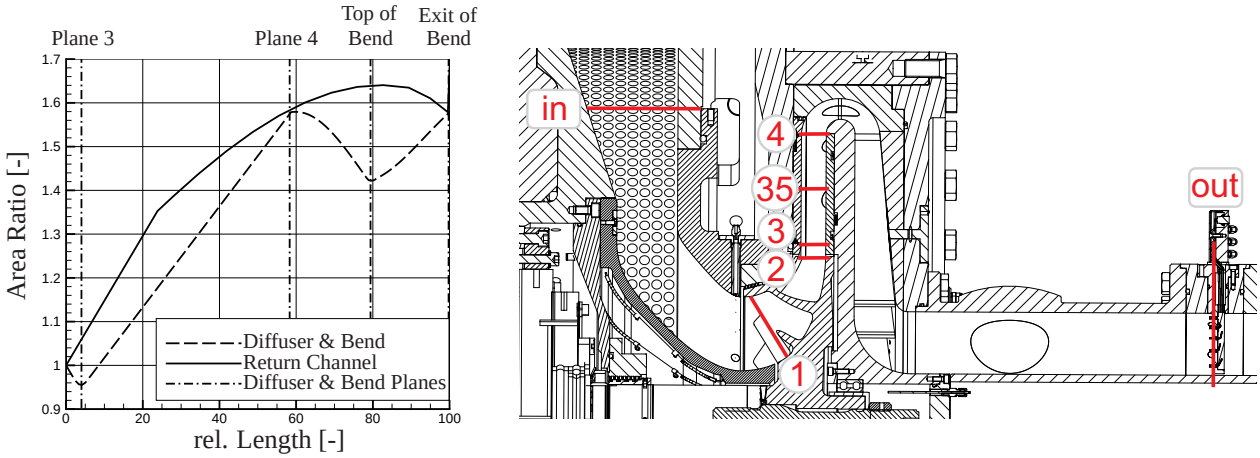

Figure 2: **Design of the diffusion system and position of measurement planes**

Measurement Concept

The performance of the stage is determined with fixed rakes in the measurement planes ”in” and ”out” (see Figure 2). The inlet conditions are measured with six circumferential equally spaced rakes with one total temperature and two total pressure probes on each rake. To accurately capture the flow state at the stage outlet, five rakes are positioned 368 mm downstream of the bend. Here, the flow is almost mixed out and a reliable integral flow state can be measured without an extensive 2D measurement traverse. These rakes are equally distributed in the circumferential direction and cover one return channel passage. To get an adequate profile over the channel height, five measurement probes are placed on each rake that divide the channel cross section in five ring elements with equal area. Three probes on each rake measure the local total pressure, one is a total temperature and one a three-hole probe, which also resolves the outlet flow angle and Mach number. By changing the position of the three-hole probe and the total temperature measurement on the rakes, a radial total temperature, outlet flow angle, static pressure, and Mach number profile can be obtained.
Additional measurement planes are added at the inlet, in the middle, and at the outlet of the diffuser to evaluate the performance of the stage components. Wall pressure data for the hub and the shroud are available in measurement plane 3 at the diffuser inlet, which is located at $r_3/r_2 = 1.075$, at plane 4 at the diffuser outlet ($r_4/r_2 = 1.75$, see Figure 2) as well as at plane 35 in the middle of the diffusor, located at $r_{35}/r_2 = 1.375$. Thus, the pressure recovery of the diffuser and the return system can be assessed separately. The total pressure in this planes can be estimated using the mass flow and the compressor head to approximate the distribution of losses to the parts of the diffusion system.

Measurement Uncertainty

The uncertainty in measurements can be divided into systematic and random errors. The propagation of uncertainty is done by the alternative error model by Grabe (2011). It is based on general Gaussian error propagation but represents a more conservative error estimate due to the linear summation of systematic deviations in contrast to the stochastic Gaussian treatment. The uncertainty of systematic and random errors of a defined quantity Φ is calculated using

$$u_{\overline{\Phi}} = \frac{t_\mathrm{p}\,(n-1)}{\sqrt{n}} \sqrt{\sum_{i=1}^{m} \left(\frac{\partial \Phi}{\partial \overline{x}_i} f_{\mathrm{r},i}\right)^2} + \sum_{i=1}^{m} \left|\frac{\partial \Phi}{\partial \overline{x}_i}\right| f_{\mathrm{s},i} \quad , \tag{2}$$

where t_p defines the student factor, n the number of samples, m the number of measured parameters, $\frac{\partial \Phi}{\partial \overline{x}_i}$ the partial derivative of Φ for a measurement parameter $\overline{x}_i$, and $f_{\mathrm{r},i}$ or $f_{\mathrm{s},i}$ the absolute random or systematic error of $\overline{x}_i$, respectively.

Mass Flow Measurement

The mass flow is measured using a venturi meter. The entire venturi meter including the upstream and downstream piping and elbows was calibrated to reduce systematic errors and increase measurement accuracy. Additionally, highly accurate differential pressure sensors with an uncertainty of 0.005% full scale and a very narrow range were applied, which led to measurement errors for the flow rate φ_{Stage} of less than $\pm$0.45%.

Wall Pressure Measurements

The wall pressure data in planes 3 and 4 are recorded by pressure taps inside the diffuser wall. The holes have a diameter of 0.4 mm and are designed as described by Shaw (1960). Uncertainty in wall pressure measurements depends on the manufacturing quality and the flow conditions. Several authors have published their reports on this topic. Rayle (1949) showed the influence of opening deviations. Since the institute's workshop has extensive experience manufacturing aerodynamic probes and sensors and the diffuser wall is straight, the systematic error is expected to be less than 0.15% of the dynamic pressure. The second error source is the position of the hole in a gradient field. A positioning error of less than 0.1 mm is expected and calculated in the pressure error by using the local pressure gradient of the operating point. The pressure gradient can be estimated with a 1D model as described in the following section. The third source is the measurement system. All pressures are measured against a reference pressure. Thus, the range of the devices could be decreased. The reference pressure is measured with a highly accurate device with an uncertainty of 0.005% full scale. The differential devices have an accuracy of 0.15% full scale. The uncertainty of the devices is also added to the error bars. The error bar of the static pressure probes ranges from 66 to 120 Pa depending on the measurement location and the operating point.

Measurement of the Outlet Conditions

The instrumentation downstream of the L-bend is designed using numerical simulations. The number and location of the probes were chosen based on this analysis to accurately capture the integral flow conditions for all operating conditions. Thus, errors caused by averaging the field could be minimized.

The outlet total temperature is measured with five pt100 sensors. The main error sources are deviations from the characteristic resistance-temperature line of the sensor, thermal conduction, the recovery factor, and the measurement chain. All sensors are calibrated, and the coefficients of the characteristic lines are determined individually in a highly stable oil bath in the institute's calibration laboratory. The thermal conduction and the recovery factor are determined in wind channel calibrations. The resulting error in the outlet temperature is $\pm$ 0.16 K.

EXPERIMENTAL RESULTS

The results were recorded at a suction pressure of $p_{\mathrm{t,in}} = 1\ \mathrm{bar}$ and a total temperature level of $T_{\mathrm{t,in}} \approx 295\ \mathrm{K}$, which corresponds to a Reynolds number of $Re = \frac{u_2 b_2}{\nu_{1,\mathrm{t}}} = 6.6 \times 10^5$ for the design conditions. The kinematic viscosity $\nu_{1,\mathrm{t}}$ was therefore calculated using Sutherland's law for the total inlet conditions. The global stage performance based on the measurement planes "in" and "out" is shown in Figures 3 and 4. As mentioned before, the stage is designed for high flow rates of $\varphi_{\mathrm{Stage}} = 0.15$ and has a wide operating range. As usual for impellers for this application, the large impeller exit angle of $\beta_2 = 130^\circ$ results in a moderate, negative slope of the work input characteristic $\Psi_{\mathrm{h,tt}}$. The characteristic is almost linear, but diminishes close to choke.

Figure 3 shows the work input coefficient $\Psi_{\mathrm{h,tt}}$ and the compressor head coefficient $\Psi_{\mathrm{y,tt}}$, which are linked by the total-to-total polytropic compressor efficiency $\eta_{\mathrm{p,tt}}$. The latter reaches its maximum

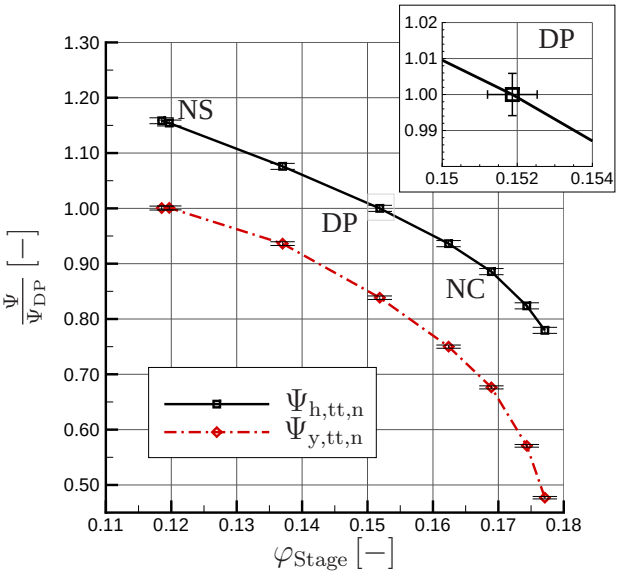

Figure 3: **Work input and compressor head**

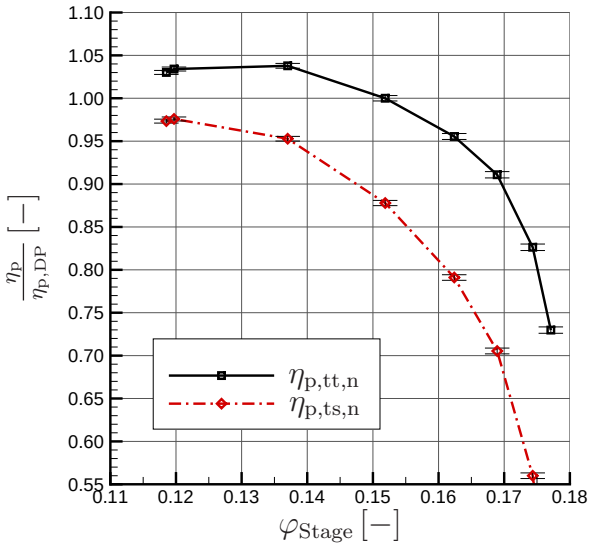

Figure 4: **Polytropic compressor efficiency**

at highly throttled operating conditions as depicted in Figure 4, and a slight efficiency drop can be observed at stall. The stage never went into stall to prevent the test rig from being damaged, and the last recorded operating point marks the end of the stable and stationary operating range. Instationarity was observed by the fluctuating total inlet and outlet pressures as well as noise.

For many applications, a specific static pressure level is required, and the kinetic energy at the compressor outlet is lost. Therefore, the total-to-static efficiency $\eta_{\mathrm{p,ts}}$ of the compressor stage is also evaluated. The efficiency is highest close to stall due to lower $p_{\mathrm{dyn,out}}/p_{\mathrm{t,out}}$ values at this operating condition. The $\eta_{\mathrm{p,ts}}$ characteristic decreases sharply as the flow rate is increased, which is the result of the negative pressure recovery C_{p} of the return channel at high flow rates, defined by

$$C_{\mathrm{p,i-j}} = \frac{p_{\mathrm{i}} - p_{\mathrm{j}}}{p_{\mathrm{t,j}} - p_{\mathrm{j}}} \quad , \tag{3}$$

as shown in the following sections.

Performance of the Stage Components

The performance of the stage components is evaluated using a 1D model of the diffuser based on wall pressure measurements at several measurement planes. The method is similar to the approach of Hausenblas (1965) and uses a correlation by Traupel (1962).

First, the flow state in a measurement plane at $r_{35}/r_2 = 1.375$, which corresponds to 50% of the diffuser length, can be determined iteratively using the average wall pressure, the measured mass flow, and the correlation for the estimated swirl loss due to wall friction by Traupel (1962). The dissipation coefficient c_{D} is set to 0.005, and the friction coefficient c_{f} is assumed to be 0.003 as proposed by Schmalfuß (1972) for diffusers with large channel heights. The influence of the radius ratio r/r_2 and the flow angle α on these coefficients, as described by Brown (1947), are neglected. It shall be mentioned that these coefficients affect the predicted losses severely. This results in uncertainty of the global loss level. However, the model can be used to identify trends between different operating points, which are discussed in this paper.

Starting from the measurement plane at $r_{35}/r_2 = 1.375$, the pressure distribution can be calculated sequentially inward to the impeller exit using Traupel's 1D approach. A chart of the calculation procedure is presented in Figure 5.

The circumferential velocity at the impeller outlet is compared to the value calculated using Euler's turbine equation. If the difference is larger than the threshold value ϵ, the sum of the calculated swirl losses from the measurement plane to the impeller outlet are used to correct the estimated flow state in the measurement plane, which leads to a new sequential calculation of the pressure field. This process is repeated until the circumferential velocity at the impeller exit matches the one calculated from Euler's turbine equation. The threshold value was $\epsilon = 0.01\,\mathrm{m/s}$, which corresponds to a $\Delta T_{\mathrm{t},2}$ of approximately $0.03\,\mathrm{K}$ and is well below the measurement accuracy of the total temperature measurements. After the iteration of the flow state in the measurement plane, the pressure buildup from this plane to the diffuser exit is calculated using the same procedure. With this 1D method, the approximate flow state including the pressure, velocity and flow angle, is known for the entire diffuser, and the performance of each stage component (impeller, diffuser, and return channel) can be assessed for different operating conditions.

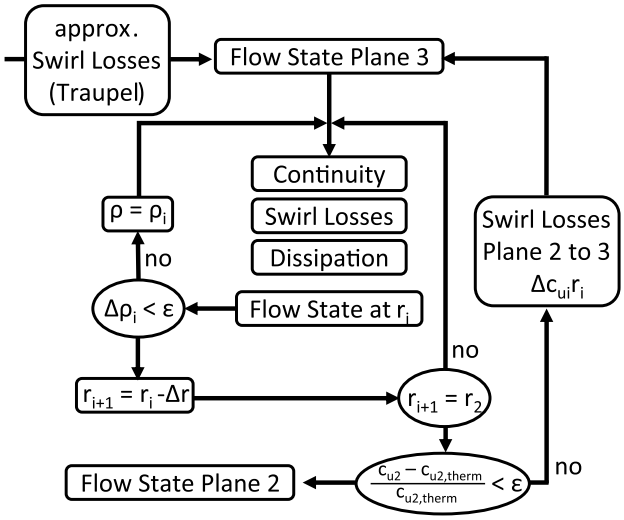

Figure 5: **Chart of the 1d Method**

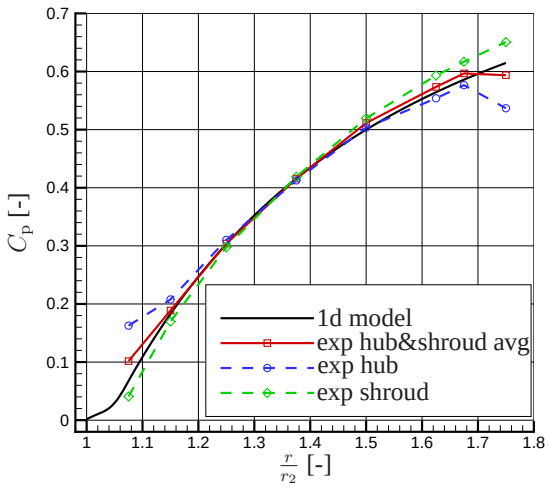

Figure 6: **Pressure distributions inside the diffuser at design conditions plotted against the diffuser radius ratio**

The 1D model predicts the pressure buildup in the middle part of the diffuser very well as shown in Figure 6. Some discrepancies are visible close to the diffuser inlet and the exit. At the diffuser inlet, the shape of the shroud-side diffuser pinch imposes a pressure gradient from the shroud to the hub due to the meridional curvature of the channel. The 1D model does not account for these curvature effects, which leads to discrepancies between the predicted and the measured average pressures at the diffuser inlet. The pressure gradient intensifies as the meridional velocity increases, which leads to larger deviations at high flow rates φ_{Stage}. A similar effect can be observed close to the diffuser exit. Here, the potential field of the U-bend decelerates the flow near the shroud and accelerates the flow near the hub. Thus, a purely one-dimensional examination of the flow is not possible close to the U-bend, and the 1D model cannot predict the average pressure at this location correctly.
Despite the uncertainties, the efficiency of the impeller with or without the diffuser can be estimated using the 1D model and can be compared to the overall stage efficiency (see Figures 7 and 8). Continuous lines refer to the values predicted by the 1D model, whereas dotted lines refer to the measured values in these graphs. The polytropic total-to-total efficiency of the impeller $\eta_{\mathrm{p,tt,in-2}}$ (from plane "in" to 2) degenerates less than the stage efficiency $\eta_{\mathrm{p,tt,in-out}}$ (from plane "in" to "out") at high flow rates as shown in Figure 7. The predicted diffuser losses decrease near choke as the friction losses decrease due to the larger flow angles at the impeller exit and the resultant shorter flow paths. This leads to a smaller efficiency drop in $\eta_{\mathrm{p,tt,in-4}}$ compared to $\eta_{\mathrm{p,tt,in-2}}$ for higher flow rates as illustrated

by the difference $^{\Delta\eta_{\mathrm{p,tt}}}/_{\eta_{\mathrm{p,tt,DP}}}$ in Figure 7. As the plot of $\eta_{\mathrm{p,tt,in-out}}$ indicates, the return channel causes a large efficiency drop compared to the efficiency of the impeller combined with the diffuser $\eta_{\mathrm{p,tt,in-4}}$. This drop increases for higher flow rates (see $^{\Delta\eta_{\mathrm{p,tt}}}/_{\eta_{\mathrm{p,tt,DP}}}$ between in-4 and in-out in Figure 7). This effect is linked to the flow angle at the inlet of the return channel. The return channel vanes are designed for an inflow angle of $\alpha_5 = 25°$. The flow angle at the diffuser exit varies between approximately $25°$ and $51°$ and is larger than $36°$ for $\varphi_{\mathrm{Stage}} > 0.14$ according to the 1D model. The flow angle changes in the cross-over bend are assumed to be small because of the unchanged cross section at the inlet and the outlet of the bend. This results in increased negative incidence angles for the return channel vanes, which cause additional losses at high flow rates. The large difference between $\eta_{\mathrm{p,tt,in-4}}$ and $\eta_{\mathrm{p,tt,in-out}}$ shows the importance of the return channel design for the overall efficiency of the stage.

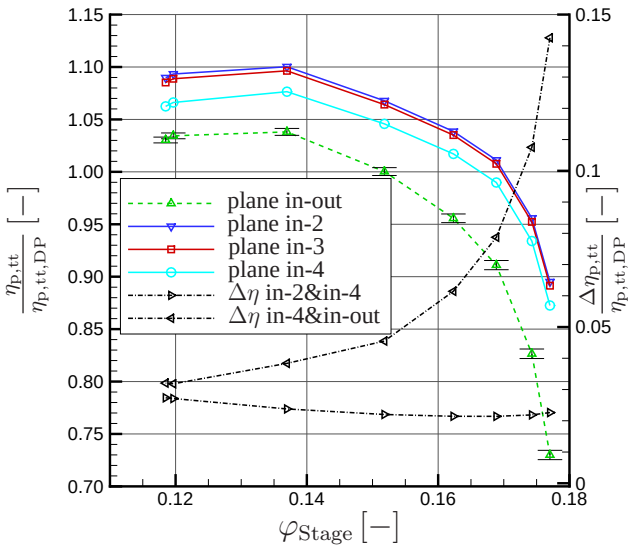

Figure 7: **Total-to-total polytropic efficiency**

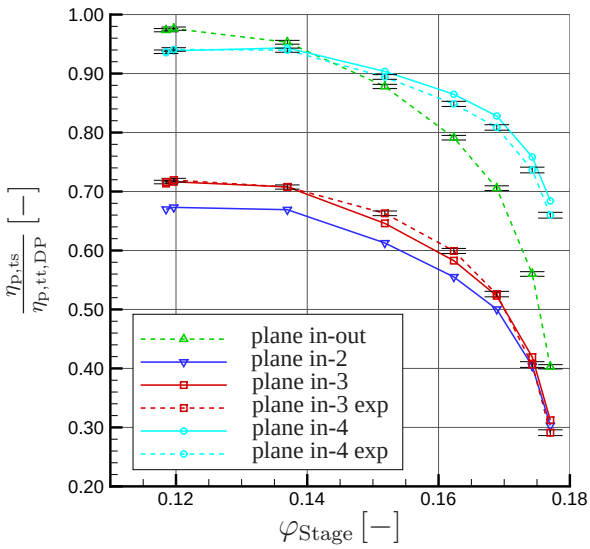

Figure 8: **Total-to-static polytropic efficiency**

The differences are even more obvious when the total-to-static efficiency is evaluated. The impeller efficiency $\eta_{\mathrm{p,ts,in-2}}$ is low (see Figure 8) due to the high velocities at the impeller outlet. The flow is decelerated in the diffuser, which leads to higher $\eta_{\mathrm{p,ts,in-3}}$ and $\eta_{\mathrm{p,ts,in-4}}$. The diffuser pinch reduces the deceleration of the meridional flow from planes 2 to 3. This results in low pressure recovery factors C_{p} at high flow rates because of the larger flow angles, as depicted in Figure 9. At low flow rates, the deceleration of the circumferential velocity u due to the radius change is dominant, which leads to larger C_{p} and $\eta_{\mathrm{p,ts,in-3}}$ values (see Figures 8 and 9). The pressure recovery of the diffuser (plane 2 to 4) is almost constant over the operating range as shown in Figure 9.

The 1D model predicts a slight drop in the pressure recovery toward lower flow rates because of the growing friction losses due to the smaller flow angles. This is not visible in the measured C_{p} values of plane 4 due to the potential field of the U-bend. The radius of curvature at the hub of the U-bend is much smaller than on the shroud side. The hub-side acceleration of the flow is therefore much stronger than the deceleration at the shroud, which decreases the average pressure in the measurement plane. Thus, the measured pressure values in plane 4 are smaller than predicted by the 1D model. As the meridional velocity increases with the increasing flow rates, this effect is more pronounced at high φ_{Stage}, which leads to decreasing measured C_{p} values as φ_{Stage} increases.

The pressure recovery of the entire diffusion system (plane 2 to out) varies significantly for different operating conditions (see Figure 9). A very low pressure recovery is observed at choke while the pressure recovery increases toward stall. This corresponds to the low total-to-static efficiency of the

stage for high flow rates as visible in Figure 8. The strong variation in $C_{\mathrm{p,2-out}}$ is caused by the pressure recovery of the return channel (plane 4 to "out"). The pressure recovery of the return channel can be calculated by subtracting the predicted pressure recovery of the diffuser $C_{\mathrm{p,2-4}}$ from $C_{\mathrm{p,2-out}}$ as shown in black in Figure 9. For large flow rates ($\varphi_{\mathrm{Stage}} > 0.14$), $C_{\mathrm{p,4-out}}$ is negative due to the negative incidence angles at the return channel vane as described above. The flow angle gets smaller as the flow rate decreases, which leads to better alignment of the flow and the return channel vanes and slightly positive pressure recovery of the return channel for low φ_{Stage} values. Thus, the total-to-static efficiency of the stage $\eta_{\mathrm{p,ts,in-out}}$ peaks at stall (see Figure 8).

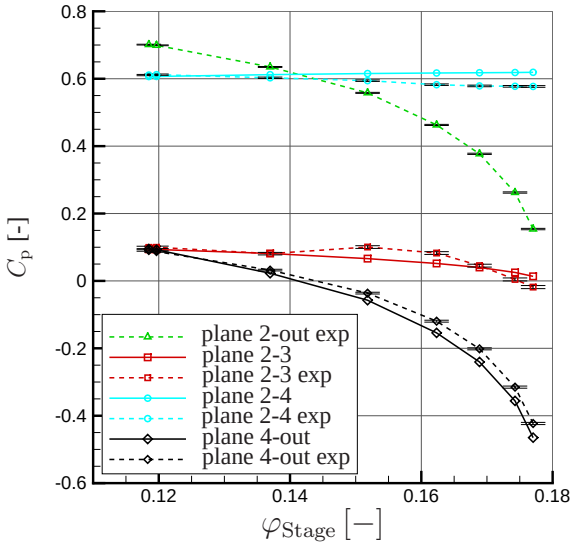

Figure 9: **Pressure recovery inside the components of the diffusion system**

Another common method for evaluating the performance of the stage components is to assess the static enthalpy rise Δh of each component. A high degree of reaction is desirable to minimize possible efficiency penalties due to stator losses. Dalbert et al. (1999) stated that industrial centrifugal compressors usually have a degree of reaction $r_{\mathrm{h,t}} = {}^{\Delta h_{\mathrm{imp}}}/_{\Delta h_{\mathrm{t}}}$ of approximately 0.6 to 0.7, where Δh_{imp} and Δh_{t} define the static enthalpy rise of the impeller and the whole stage, respectively.
The degree of reaction is defined as $r_{\mathrm{h,t}} = {}^{\Delta h_{\mathrm{ts,imp}}}/_{\Delta h_{\mathrm{t}}}$ as shown in Figure 10. It is below the range stated by Dalbert because it also accounts for the kinetic energy at the impeller inlet. The impeller slip $c_{\mathrm{slip}} = c_{\mathrm{u2\,inf}} - c_{\mathrm{u2}}$ remains almost constant for $\varphi_{\mathrm{Stage}} < 0.165$, but rises toward choke by approximately 9%, which corresponds to a change in the relative outlet flow angle β_2 of about 4.6° according to the 1D model. The change in the relative flow angle combined with the changing meridional velocity leads to almost constant impeller exit velocities c_2, which can be obtained from the velocity triangles for the impeller exit. The total degree of reaction diminishes near choke as the kinetic energy at the impeller exit remains almost constant for the entire operating range. The pressure recovery in the diffuser is also almost constant for all operating points as shown in Figure 9. An almost identical static enthalpy rise $\Delta h_{\mathrm{ss,diff}}$ for all operating points is caused by the constant deceleration in the diffuser. As $\Psi_{\mathrm{h,tt}}$ decreases for high flow rates, the share of the static enthalpy increase in the diffuser ${}^{\Delta h_{\mathrm{ss,diff}}}/_{\Delta h_{\mathrm{t}}}$ rises towards choke as shown in Figure 10. The remaining kinetic energy at the diffuser exit is between 11% and 17% of the total enthalpy increase for the stage. The rise of ${}^{c_4^2}/_{2\Delta h_{\mathrm{t}}}$ toward choke is caused by the higher meridional velocity and a decreasing $\Psi_{\mathrm{h,tt}}$. Ribi (2007) evaluated diffuser exit velocities for multiple compressors and stated that ${}^{c_4^2}/_{u_2^2} \approx 0.16$ can be expected for high flow stages. The current stage has a large diffuser outlet diameter that leads to values of ${}^{c_4^2}/_{u_2^2} \approx 0.14$ for the entire speedline.

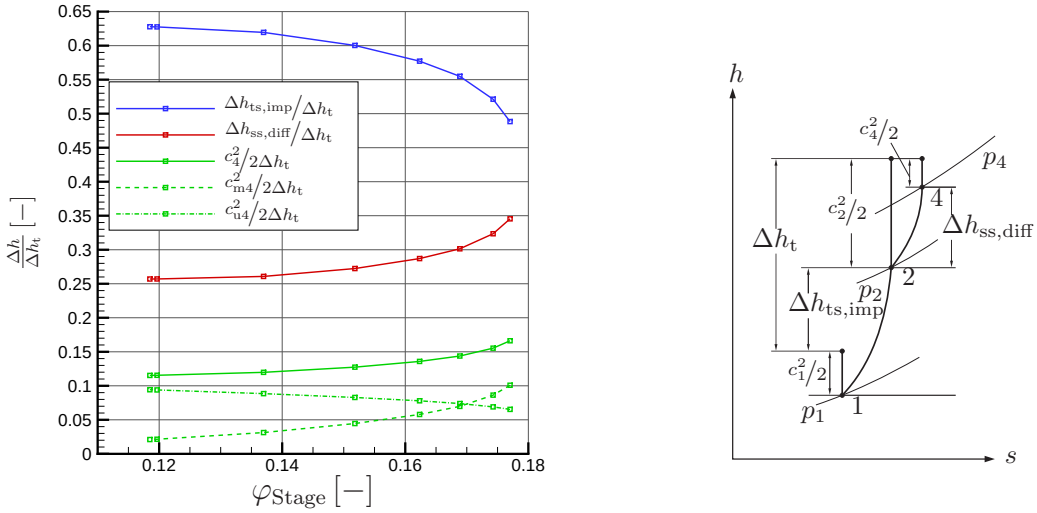

Figure 10: **Change of enthalpy inside the stage components**

Flow Conditions at the Stage Outlet

Figure 11 shows the total pressure and the outlet angle distribution for five channel heights at the stage outlet (plane ”out”) and the three operating points highlighted in Figure 3. They include a point near choke (NC), the design point (DP), and one near stall (NS). The total pressure values are circumferential and mass-flow averaged. They show a significant trend from higher total pressure at the hub to lower at the shroud for all operating points. This profile results from the detachment of the flow at the shroud side downstream of the L-turn. This blockage forces the fluid toward the hub and accelerates the flow. The higher velocity at the hub leads to high total pressure while total pressure losses due to the detachment decrease the total pressure at the shroud. The size of the detachment increases for higher flow rates, i.e. from NC to NS, which strengthens the blockage effects. Thus, the gradient of the total pressure increases from lower to higher flow rates. The plots of α in Figure 11 show the distribution of the velocity vector in the circumferential direction for the three operating points, while the meridional component is free of swirl.

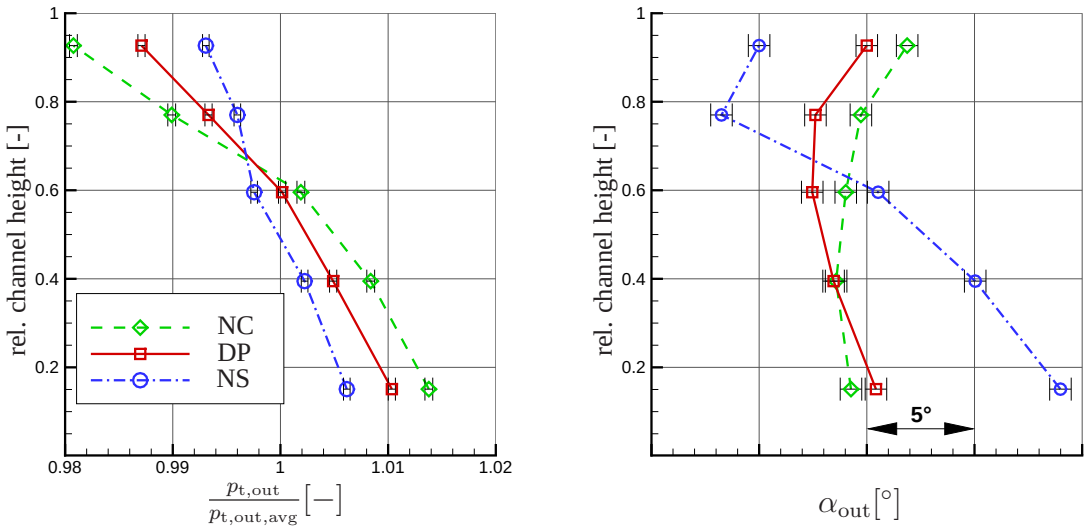

Figure 11: **Stage Outlet: total pressure (left) and flow angle (right)**

The characteristics for NC and DP describe a well-balanced α distribution across the channel height. In contrast, the near stall state has an inhomogeneous distribution from the hub to the shroud resulting from the flow inside the return channel. Numerical investigations showed a blockage at the suction side of the vanes at the shroud occurring particularly for lower flow rates (NS) and an inflow with low incidence. This blockage reduces the redirection of the flow and accordingly leads to smaller outlet flow angles at the shroud. In contrast, the negative pressure gradient at the hub near the vane outlet ensures a very well follow behavior of the flow through the return channel near the hub. Since the material angle turns the flow in a counter-swirl, the fluid also leaves the return channel in a counter-swirl at the hub. The counter-swirl is further increased by deceleration of the flow in the meridional direction inside the L-turn, which explains the high outlet flow angles near the hub. Unfortunately, these effects have not been verified with experimental measurements so far, but will in future work.

CONCLUSIONS

A test rig for stages of centrifugal process compressors was set up at RWTH Aachen University and has been described in this paper. The measurement concept was presented, and the first experimental results were shown, which include global stage performance data and stage efficiencies. Based on these measurement results, a 1D model of the diffuser was used to evaluate the performance behavior of the stage components. The negative impact of the return channel on the stage efficiency and pressure recovery at high flow rates was identified. The steeper flow angle in the diffuser for high flow rates leads to increased negative incidence at the return channel inlet. This results in severe losses due to secondary flow and a negative pressure recovery.
An open test case will be published based on the presented and future experimental results of the stage currently investigated, which shall be used to validate numerical methods and turbulence modeling.

ACKNOWLEDGEMENTS

The authors would like to thank the European Union's European Regional Development Fund (ERDF) for funding the Project 'Hightech.NRW Process Centrifugal Compressor' within the NRW 'Ziel 2-Programm'. Furthermore, we thank MAN Diesel & Turbo SE (Oberhausen) for providing the geometries and supporting the project.

References

Aalburg, C., Sezal, I., Haigermoser, C., Simpson, A., Michelassi, V., and Sassanelli, G. (2011). Annular Cascade for Radial Compressor Development. *ASME, Paper No. GT2011-468734*.

Aalburg, C., Simpson, A., Schmitz, M. B., Michelassi, V., Evangelisti, S., Belardini, E., and Ballarini, V. (2008). Design and Testing of Multistage Centrifugal Compressors with Small Diffusion Ratios. *Proceedings of ASME Turbo Expo 2008: Power for Land, Sea and Air; GT2008-51263*.

Brown, B. (1947). Friction Coefficients in a Vaneless Diffuser. *NACA Technical Note*, 1311.

Dalbert, P., Ribi, B., Kmeci, T., and Casey, M. V. (1999). Radial Compressor Design for industrial Compressors. *Proceedings of the Institution of Mechanical Engineers*, 213 Part C:71–83.

Grabe, M. (2011). *Grundriss der generalisierten Gauß'schen Fehlerrechnung*. Springer Heidelberg.

Hausenblas, H. (1965). Trennung der Lauf- und Leitradverluste bei der Auswertung von Versuchen an einstufigen Radialverdichtern. *Forschung im Ingenieurwesen*, 31(1):11–13.

Hildebrandt, A. (2011). Aerodynamic Optimisation of a Centrifugal Compressor Return Channel and U-turn with Genetic Algorithms. In *Proceedings of ASME Turbo Expo 2011, GT2011-450876*.

Inoue, Y. and Koizumi, T. (1983). An experimental Study on the Flow Patterns and Losses in Return Passages for Centrifugal Compressors. Applied Mechanics, Bioengineering and Fluid Engineering Conference, Houston.

Lenke, J. (1999). *Numerische Simulation der turbulenten Strömung in Rückführkanälen mehrstufiger Radialverdichter*. PhD thesis, Gerhard-Mercator Universität Duisburg.

Lenke, J. and Simon, H. (1998). Numerical Simulation of the Flow through the Return Channel of Multi-stage Centrifugal Compressors. *Transaction of the ASME, Paper No. 98-GT-255*.

Lenke, J. and Simon, H. (1999). Numerical Investigations on the Optimum Design of Return Channel of Multi-Stage Centrifugal Compressor. *Transaction of the ASME, Paper No. 99- GT-103*.

Rayle, R. (1949). An Investigation of the Influence of Crifice Geometry on static Pressure Measurement. Master's thesis, Massachusetts Institute of Technology.

Reutter, O., Hildebrandt, A., Jakiel, C., Raitor, T., and Voss, C. (2011). Automated Aerodynamic Optimization of a Return Channel Vane of a multistage Compressor. 9th European Conference on Turbomachinery Fluid Dynamics and Thermodynamics, Paper No. 45.

Ribi, B. (2007). Turbomachinery Design. Lecture Series ETH Zürich.

Rothstein, E. (1984). *Experimentelle und theoretische Untersuchung der Strömungsvorgänge in Rückführkanälen von Radialverdichterstufen, insbesondere solcher mit geringen Kanalbreiten*. PhD thesis, Rheinisch-Westfälische Technische Hochschule Aachen.

Rothstein, E. and Gallus, H. (1983). Untersuchung von beschaufelten Rückführkanälen mehrstufiger Radialverdichter. VDI-Berichte 487.

Schmalfuß, H. G. (1972). Strömung in parallelwandigen Radialdiffusoren. *Zeitschrift für Flugwissenschaften*, 20:22–26.

Schmitz, M., Simpson, A., Aalburg, C., and Michelassi, V. (2008). Development of a Sector Test Rig For Multistage Radial Compressor Stators. International Symposium on Transport Phenomena and Dynamics of Rotating Machinery.

Shaw, R. (1960). The influence of hole dimensions on static pressure measurements. *Journal of Fluid Mechanics*, 7(04):550–564.

Simon, H. and Rothstein, E. (1983). On the Development of Return Passages of Multi-Stage Centrifugal Compressors. Bioengineering and Fluids Engineering Conference.

Simpson, A., Aalburg, C., Schmitz, M., Pannekeet, R., Larisch, F., and Michelassi, V. (2008). Design, Validation and Application of a Radial Cascade for Centrifugal Compressors. *Proceedings of ASME Turbo Expo 2008: Power for Land, Sea and Air; Paper No. GT2008-51262*.

Traupel, W. (1962). *Die Theorie der Strömung durch Radialmaschinen*. Verlag G. Braun, Karlsruhe.